Research Article | Vol. 26, No. 3 | 5 Feb 2018 | OPTICS EXPRESS 3684
Optics EXPRESS

Megawatt peak power tunable femtosecond source based on self-phase modulation enabled spectral selection

HSIANG-YU CHUNG,[1,2] WEI LIU,[1,2] QIAN CAO,[1,2] LIWEI SONG,[1,3] FRANZ X. KÄRTNER,[1,2,4] AND GUOQING CHANG[1,4,*]

[1]*Center for Free-Electron Laser Science, DESY, Notkestraße 85, 22607 Hamburg, Germany*
[2]*Physics Department, Universität Hamburg, Luruper Chaussee 149, 22761 Hamburg, Germany*
[3]*State Key Laboratory of High Field Laser Physics, Shanghai Institute of Optics and Fine Mechanics, Chinese Academy of Sciences, 201800 Shanghai, China*
[4]*The Hamburg Centre for Ultrafast Imaging, Universität Hamburg, Luruper Chaussee 149, 22761 Hamburg, Germany*
**guoqing.chang@desy.de*

Abstract: Wavelength widely tunable femtosecond sources can be implemented by optically filtering the leftmost/rightmost spectral lobes of a broadened spectrum due to self-phase modulation (SPM) dominated fiber-optic nonlinearities. We numerically and experimentally investigate the feasibility of implementing such a tunable source inside optical fibers with negative group-velocity dispersion (GVD). We show that the spectral broadening prior to soliton fission is dominated by SPM and generates well-isolated spectral lobes; filtering the leftmost/rightmost spectral lobes results in energetic femtosecond pulses with the wavelength tuning range more than 400 nm. Employing an ultrafast Er-fiber laser and a dispersion-shifted fiber with negative GVD, we implement an energetic tunable source that produces ~100-fs pulses tunable between 1.3 μm and 1.7 μm with up to ~16-nJ pulse energy. Further energy scaling is achieved by increasing the input pulse energy to ~1-μJ and reducing the fiber length to 1.3 cm. The resulting source can produce >100-nJ femtosecond pulses at 1.3 μm and 1.7 μm with MW level peak power, representing an order of magnitude improvement of our previous results. Such a powerful source covers the 2nd and the 3rd biological transmission window and can facilitate multiphoton deep-tissue imaging.

OCIS codes: (060.7140) Ultrafast processes in fibers; (060.4370) Nonlinear optics, fibers.

References and links

1. M. E. Fermann and I. Hartl, "Ultrafast fibre lasers," Nat. Photonics **7**(11), 868–874 (2013).
2. D. Brida, G. Krauss, A. Sell, and A. Leitenstorfer, "Ultrabroadband Er:fiber lasers," Laser Photonics Rev. **8**(3), 409–428 (2014).
3. H. Lim, J. Buckley, A. Chong, and F. W. Wise, "Fibre-based source of femtosecond pulses tunable from 1.0 to 1.3 μm," Electron. Lett. **40**(24), 1523–1525 (2004).
4. F. Tauser, F. Adler, and A. Leitenstorfer, "Widely tunable sub-30-fs pulses from a compact erbium-doped fiber source," Opt. Lett. **29**(5), 516–518 (2004).
5. J. Takayanagi, T. Sugiura, M. Yoshida, and N. Nishizawa, "1.0–1.7-μm wavelength-tunable ultrashort-pulse generation using femtosecond Yb-doped fiber laser and photonic crystal fiber," IEEE Photonics Technol. Lett. **18**(21), 2284–2286 (2006).
6. J. van Howe, J. H. Lee, S. Zhou, F. Wise, C. Xu, S. Ramachandran, S. Ghalmi, and M. F. Yan, "Demonstration of soliton self-frequency shift below 1300 nm in higher-order mode, solid silica-based fiber," Opt. Lett. **32**(4), 340–342 (2007).
7. K. Wang and C. Xu, "Tunable high-energy soliton pulse generation from a large-mode-area fiber and its application to third harmonic generation microscopy," Appl. Phys. Lett. **99**(7), 071112 (2011).
8. M. E. V. Pedersen, J. Cheng, K. Charan, K. Wang, C. Xu, L. Grüner-Nielsen, and D. Jakobsen, "Higher-order-mode fiber optimized for energetic soliton propagation," Opt. Lett. **37**(16), 3459–3461 (2012).
9. J. Lim, H.-W. Chen, S. Xu, Z. Yang, G. Chang, and F. X. Kärtner, "3 GHz, watt-level femtosecond Raman soliton source," Opt. Lett. **39**(7), 2060–2063 (2014).
10. S. R. Domingue and R. A. Bartels, "Three-photon excitation source at 1250 nm generated in a dual zero dispersion wavelength nonlinear fiber," Opt. Express **22**(25), 30777–30785 (2014).

#315516 https://doi.org/10.1364/OE.26.003684
Journal © 2018 Received 12 Dec 2017; revised 29 Jan 2018; accepted 30 Jan 2018; published 2 Feb 2018

Optics EXPRESS

11. K. Wang, N. G. Horton, K. Charan, and C. Xu, "Advanced fiber soliton sources for nonlinear deep tissue imaging in biophotonics," IEEE J. Sel. Top. Quantum Electron. **20**(2), 6800311 (2014).
12. J. W. Nicholson, A. Desantolo, W. Kaenders, and A. Zach, "Self-frequency-shifted solitons in a polarization-maintaining, very-large-mode area, Er-doped fiber amplifier," Opt. Express **24**(20), 23396–23402 (2016).
13. L. Rishoj, B. Tai, P. Kristensen, and S. Ramachandran, "Characterization of Intermodal Group Index Matched Soliton Interactions leading to MW Peak Powers at 1300 nm," in Conference on Lasers and Electro-Optics, OSA Technical Digest (online) (Optical Society of America, 2017), paper STh3K.2.
14. P. Cadroas, L. Abdeladim, L. Kotov, M. Likhachev, D. Lipatov, D. Gaponov, A. Hideur, M. Tang, J. Livet, W. Supatto, E. Beaurepaire, and S. Février, "All-fiber femtosecond laser providing 9 nJ, 50 MHz pulses at 1650 nm for three-photon microscopy," J. Opt. **19**(6), 065506 (2017).
15. H.-W. Chen, Z. Haider, J. Lim, S. Xu, Z. Yang, F. X. Kärtner, and G. Chang, "3 GHz, Yb-fiber laser-based, few-cycle ultrafast source at the Ti:sapphire laser wavelength," Opt. Lett. **38**(22), 4927–4930 (2013).
16. H. Tu, J. Lægsgaard, R. Zhang, S. Tong, Y. Liu, and S. A. Boppart, "Bright broadband coherent fiber sources emitting strongly blue-shifted resonant dispersive wave pulses," Opt. Express **21**(20), 23188–23196 (2013).
17. M.-C. Chan, C.-H. Lien, J.-Y. Lu, and B.-H. Lyu, "High power NIR fiber-optic femtosecond Cherenkov radiation and its application on nonlinear light microscopy," Opt. Express **22**(8), 9498–9507 (2014).
18. X. Liu, A. S. Svane, J. Lægsgaard, H. Tu, S. A. Boppart, and D. Turchinovich, "Progress in Cherenkov femtosecond fiber lasers," J. Phys. D Appl. Phys. **49**(2), 023001 (2016).
19. J. P. Epping, M. Kues, P. J. M. van der Slot, C. J. Lee, C. Fallnich, and K. J. Boller, "Integrated CARS source based on seeded four-wave mixing in silicon nitride," Opt. Express **21**(26), 32123–32129 (2013).
20. T. Gottschall, T. Meyer, M. Schmitt, J. Popp, J. Limpert, and A. Tünnermann, "Four-wave-mixing-based optical parametric oscillator delivering energetic, tunable, chirped femtosecond pulses for non-linear biomedical applications," Opt. Express **23**(18), 23968–23977 (2015).
21. M. Brinkmann, S. Dobner, and C. Fallnich, "Light source for narrow and broadband coherent Raman scattering microspectroscopy," Opt. Lett. **40**(23), 5447–5450 (2015).
22. R. H. Stolen and C. Lin, "Self-phase-modulation in silica optical fibers," Phys. Rev. A **17**(4), 1448–1453 (1978).
23. P. Mamyshev, "All optical data regeneration based on self-phase modulation effect," ECOC **98**, 475–476 (1998).
24. T. Her, G. Raybon, and C. Headley, "Optimization of pulse regeneration at 40 Gb/s based on spectral filtering of self-phase modulation in fiber," IEEE Photonics Technol. Lett. **16**(1), 200–202 (2004).
25. L. Fu, M. Rochette, V. Ta'eed, D. Moss, and B. Eggleton, "Investigation of self-phase modulation based optical regeneration in single mode As_2Se_3 chalcogenide glass fiber," Opt. Express **13**(19), 7637–7644 (2005).
26. R. Lehneis, A. Steinmetz, J. Limpert, and A. Tünnermann, "All-fiber pulse shortening of passively Q-switched microchip laser pulses down to sub-200 fs," Opt. Lett. **39**(20), 5806–5809 (2014).
27. W. Fu, L. G. Wright, and F. W. Wise, "High-power femtosecond pulses without a modelocked laser," Optica **4**(7), 831–834 (2017).
28. J. Buldt, M. Müller, R. Klas, T. Eidam, J. Limpert, and A. Tünnermann, "Temporal contrast enhancement of energetic laser pulses by filtered self-phase-modulation-broadened spectra," Opt. Lett. **42**(19), 3761–3764 (2017).
29. K. Regelskis, J. Želudevičius, K. Viskontas, and G. Račiukaitis, "Ytterbium-doped fiber ultrashort pulse generator based on self-phase modulation and alternating spectral filtering," Opt. Lett. **40**(22), 5255–5258 (2015).
30. Z. Liu, Z. M. Ziegler, L. G. Wright, and F. W. Wise, "Megawatt peak power from a Mamyshev oscillator," Optica **4**(6), 649–654 (2017).
31. W. Liu, C. Li, Z. Zhang, F. X. Kärtner, and G. Chang, "Self-phase modulation enabled, wavelength-tunable ultrafast fiber laser sources: an energy scalable approach," Opt. Express **24**(14), 15328–15340 (2016).
32. W. Liu, S.-H. Chia, H.-Y. Chung, R. Greinert, F. X. Kärtner, and G. Chang, "Energetic ultrafast fiber laser sources tunable in 1030-1215 nm for deep tissue multi-photon microscopy," Opt. Express **25**(6), 6822–6831 (2017).
33. H.-Y. Chung, W. Liu, Q. Cao, F. X. Kärtner, and G. Chang, "Er-fiber laser enabled, energy scalable femtosecond source tunable from 1.3 to 1.7 μm," Opt. Express **25**(14), 15760–15771 (2017).
34. L. Shi, L. A. Sordillo, A. Rodríguez-Contreras, and R. Alfano, "Transmission in near-infrared optical windows for deep brain imaging," J. Biophotonics **9**(1-2), 38–43 (2016).
35. N. G. Horton, K. Wang, D. Kobat, C. G. Clark, F. W. Wise, C. B. Schaffer, and C. Xu, "*In vivo* three-photon microscopy of subcortical structures within an intact mouse brain," Nat. Photonics **7**(3), 205–209 (2013).
36. D. G. Ouzounov, T. Wang, M. Wang, D. D. Feng, N. G. Horton, J. C. Cruz-Hernández, Y.-T. Cheng, J. Reimer, A. S. Tolias, N. Nishimura, and C. Xu, "*In vivo* three-photon imaging of activity of GCaMP6-labeled neurons deep in intact mouse brain," Nat. Methods **14**(4), 388–390 (2017).
37. J. M. Dudley, G. Gentry, and S. Coen, "Supercontinuum generation in photonic crystal fiber," Rev. Mod. Phys. **78**(4), 1135–1184 (2006).
38. G. P. Agrawal, *Nonlinear Fiber Optics*, 5th ed. (Elsevier, 2013).

1. Introduction

Femtosecond laser sources with the center wavelength tunable in a wide range of 100s of nanometer are desired in many microscopy and spectroscopy applications. Unfortunately

Optics EXPRESS

mode-locked femtosecond lasers show only a limited tuning range due to finite gain bandwidth of laser media. As a result, nonlinear wavelength conversion has become the standard technique to achieve femtosecond pulses in the wavelength ranges that cannot be covered by mode-locked lasers. A typical solution is a mode-locked laser plus a synchronously pumped solid-state optical parametric oscillator. Recent years have seen tremendous progress in developing mode-locked fiber (e.g., Yb-doped, Er-doped, Tm-doped etc.) lasers [1,2]. Compatible with fiber technology, use of nonlinear fiber-optic methods to generate wavelength widely tunable femtosecond pulses from an ultrafast fiber laser is of particular interest. The typical methods include soliton self-frequency shift [3–14], dispersive wave generation [15–18], and four-wave mixing [19–21].

Among many nonlinear fiber-optic phenomena, self-phase modulation (SPM) itself can also broaden an optical spectrum [22] to generate new wavelength. In 1998, Mamyshev proposed to use SPM-induced spectral broadening followed by offset spectral filtering for optical data regeneration [23]. The resulting optical pulse reshaping can be used in optical communications to suppress the noise in "zeros" and the amplitude fluctuations in "ones" [24,25]. In these applications, long (>10s of meters) optical fibers are required because the input pulses are several picosecond in duration with ~1-W level peak power. In recent years, the idea of Mamyshev regenerator has been revived in the field of femtosecond pulse generation. For example, it allows generation of femtosecond pulses using picosecond Q-switched laser [26] or gain-switched laser [27]; it is also used to enhance the temporal contrast of mJ femtosecond pulses [28]. Incorporation of Mamyshev regenerator inside a laser cavity has resulted in a new type of mode-locked lasers [29,30].

In all above applications, SPM-induced spectral broadening increases the input spectral bandwidth by ~50 nm at most such that the regenerated pulse after optical filtering has a center wavelength close (<30 nm) to the initial pulse prior to the spectral broadening. This ensures that the regenerated pulse can be further amplified by the same gain medium that is used to amplify the initial pulse. Recently we extended the idea underlying Mamyshev regenerator and applied it to implementing wavelength widely tunable (~400 nm) femtosecond sources [31–33]. The essence of the idea is to employ SPM-dominated nonlinearity to dramatically broaden an input narrowband optical spectrum to a spectral width of 100s of nm. The resulting broadened spectrum features isolated spectral lobes with a considerable portion of power contained by the leftmost and the rightmost spectral lobes. Using optical filters to select the leftmost/rightmost spectral lobes produces nearly transform-limited ~100-fs pulses with the center wavelength widely tunable.

This new application is clearly distinct from the conventional Mamyshev regenerator in that the filtered pulses may have the center wavelength far from the initial pulse's center wavelength, leading to a wide tuning range of ~400 nm. For example, using an ultrafast Yb-fiber laser at 1030 nm as the source laser, this SPM-enabled spectral selection (SESS) allows generation of ~100-fs nearly transform-limited pulses (without external compression), tunable from 825 nm to 1210 nm with >1-nJ pulse energy [31]. SESS exhibits superior energy scalability; the resulting pulse energy can be scaled up by using shorter fibers with larger mode area. For example, SESS enabled by 2-cm large-mode-area (LMA) fiber allowed us to obtain energetic tunable pulses from an ultrafast Yb-fiber laser; the resulting pulses are tunable in the wavelength range of 1030-1215 nm with up to >20-nJ pulse energy [32]. We employed such a powerful source to multiphoton microscopy imaging of human skin [32]. We also applied SESS to ultrafast Er-fiber lasers at 1.55 μm and obtained femtosecond pulses tunable from 1.3 μm to 1.7 μm [33]. The filtered spectra at 1.3 μm and 1.7 μm correspond to two optical transmission windows and are of importance for deep-tissue imaging [34–36].

It is noteworthy that group-velocity dispersion (GVD) plays an important role to achieve efficient SESS. Pure SPM can produce a broadened spectrum with well-isolated spectral lobes and the leftmost/rightmost spectral lobe includes more power than other lobes. However, interplay between SPM and GVD tends to wash out the spectral lobes, leading to

Optics EXPRESS

reduced pulse energy for the filtered pulses. In all the previous demonstrations, we performed SESS always in optical fibers with either positive GVD or close-to-zero GVD. To mitigate the detrimental effects caused by GVD, we use short fibers (<10 cm) to achieve spectral broadening, which guarantees that SPM dominates the broadening process.

Most conventional optical fibers—especially fused silica LMA fibers—exhibit positive GVD at the Yb-fiber laser wavelength (i.e., ~1030 nm) and negative GVD at the Er-fiber laser wavelength (i.e., ~1.55 μm). Specially designed fibers at the expense of the fiber mode area may possess close-to-zero or even positive GVD at the Er-fiber laser wavelength. For example, we employed 4-cm dispersion-compensating fiber—which has a GVD of 48.5 fs^2/mm at 1.55 μm—to implement SESS and generated ~10-nJ, <100-fs pulses at 1.35 μm and 1.7 μm [33]. To scale the pulse energy to >100 nJ and therefore achieve ~1-MW peak power—a power level required by applications such as deep-tissue bioimaging [35,36], the fiber length should be reduced to ~4 mm, which becomes challenging for experimental handling. In addition, the small mode-field diameter (MFD) (6 μm for this dispersion-compensating fiber) degrades the system robustness when free-space coupling is adopted. As we have shown, energy scaling can be also achieved by increasing the MFD of an optical fiber with positive GVD [32]. At the Er-fiber laser wavelength, however, increasing the fiber MFD normally leads to negative GVD that complicates the nonlinear propagation of an ultrashort pulse inside the fiber. The negative GVD and strong SPM can reshape the input pulse into a higher-order optical soliton. Due to higher-order effects such as third-order dispersion (TOD), self-steepening, and stimulated Raman scattering, this higher-order soliton breaks into multiple fundamental solitons and emits dispersive waves; further propagation leads to wavelength red-shifted Raman solitons [37].

Ultrashort pulse propagation inside an optical fiber with negative GVD has been extensively investigated under the context of higher-order soliton pulse compression, supercontinuum generation, and soliton self-frequency shift [38]. It remains unclear whether optical fibers with negative GVD allows to implement SESS because efficient SESS requires the formation of well-isolated spectral lobes with a considerable portion of power concentrated in the leftmost/rightmost spectral lobes.

In this paper, we report the first—to the best of our knowledge—systematic investigation of the interplay between SPM and negative GVD in terms of spectral lobe formation, wavelength tunability of the filtered pulses, power conversion efficiency to the leftmost/rightmost spectral lobes, and energy scalability of the resulting tunable source. We show both numerically and experimentally that, prior to soliton fission, higher-order soliton formation compresses the input pulse and enhances the spectral broadening. The spectral broadening is still dominated by SPM and generates well-isolated spectral lobes. We find that more power is distributed in the leftmost and rightmost spectral lobes compared with SESS under positive GVD, implying that negative-GVD enabled SESS exhibits higher energy conversion efficiency. Our simulation results are verified by experiments. We first use a 31-MHz ultrafast Er-fiber laser as the pump source to excite SPM-dominated spectral broadening inside an optical fiber with −10 fs^2/mm GVD and 10-μm MFD. By filtering the leftmost or rightmost spectral lobes, we produce ~100-fs (nearly transform-limited) pulses tunable from 1.3 μm to 1.7 μm with up to >15-nJ pulse energy. To show the superior energy scalability of SESS enabled by fiber with negative GVD, we replace the Er-fiber laser by a high-energy optical parametric amplifier (OPA) as the pump source; the resulting ~100-fs pulses are tunable from 1.3 μm to 1.7 μm with >100-nJ pulse energy, corresponding to ~MW peak power. These results represent an order of magnitude improvement of our previous results in terms of pulse energy and peak power, making the high-energy SESS source attractive for deep-tissue imaging applications.

Optics EXPRESS

2. Numerical simulation

We solve the generalized nonlinear Schrödinger equation to investigate the effect of GVD on the spectral broadening at the pump wavelength of 1.55 μm. Without loss of generality, we propagate an ultrashort pulse inside three fibers featuring positive (10 fs^2/mm), zero (0 fs^2/mm), and negative GVD (–10 fs^2/mm) at 1.55 μm, respectively. To be more practical, we assume constant TOD of 100 fs^3/mm at 1.55 μm for all three cases. The input pulse (center wavelength at 1.55 μm) has a hyperbolic-secant shape with 300-fs pulse duration and 95-nJ pulse energy. We assume that these three fibers have the same MFD of 10 μm.

Figure 1(a) and 1(d) show the optical spectral and temporal evolution of the input pulse propagating inside the fiber with 10 fs^2/mm GVD. As we expect, SPM dominates the spectral broadening and forms well-separated spectral lobes [Fig. 1(a)]. Due to the positive GVD, the input pulse is stretched along the propagation distance [Fig. 1(d)]. In contrast, for propagation in the fiber with zero GVD, the pulse duration shown in Fig. 1(e) remains almost constant; consequently the broadened spectrum in Fig. 1(b) becomes broader than achieved in the fiber with positive GVD.

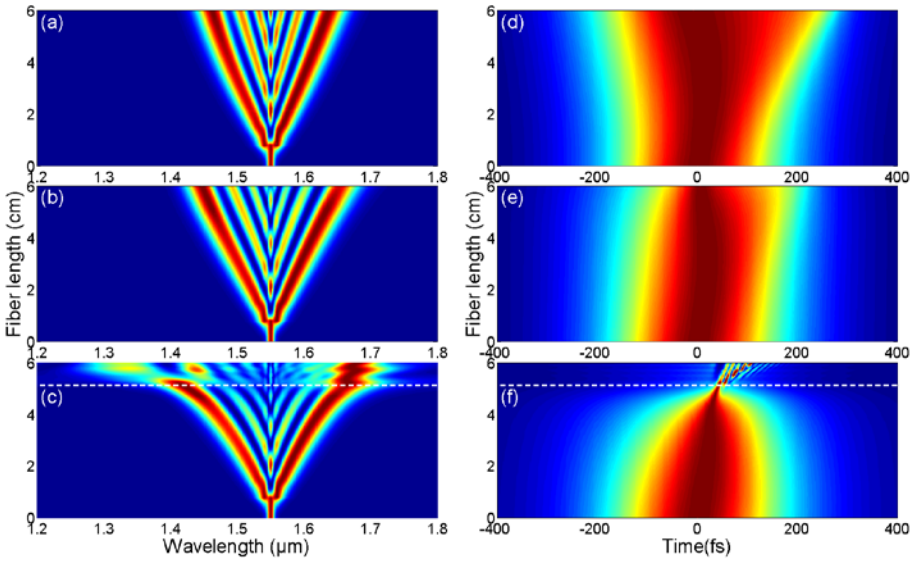

Fig. 1. Simulation results of the optical spectral (a-c) and temporal (d-f) evolution of a 300-fs, 95-nJ pulse centered at 1.55 μm propagating in optical fibers with 10-μm MFD and different GVD at 1.55 μm: 10 fs^2/mm for (a,d), 0 fs^2/mm for (b,e), and –10 fs^2/mm for (c,f). The white dashed curve denotes the soliton fission length of 5.2 cm.

Figure 1(c) and 1(f) depict the spectral and temporal evolution as the input pulse propagates in the fiber with negative GVD of –10 fs^2/mm. Due to higher-order soliton pulse compression arising from the interaction between SPM and negative GVD, the input pulse becomes shorter along the fiber length [Fig. 1(f)]. It reaches the shortest pulse duration at the fiber length of 5.2 cm, which is defined as the soliton fission length and denoted by the white dashed lines in Fig. 1(c) and 1(f). Further propagation leads to soliton fission that ejects multiple pulses, which starts to destroy the well-separated spectral lobes that originate from SPM-dominated spectral broadening.

To visualize more details, we plot in Fig. 2 the spectra and temporal pulses at fiber lengths of 4.6 cm (blue curves) and 5 cm (red dashed curves). For a comparison, we plot in the same figure the spectrum and pulse at the fiber input (black curves). Clearly the input spectrum shown as the black curve in Fig. 2(a) is substantially broadened and extended to both the short and long wavelength side. In the time domain, the pulse experiences accelerated compression; the peak power increases from 279 kW to 530 kW after propagation of 4.6 cm.

Optics EXPRESS

Then at further propagation of 0.4 cm, the peak power reaches 893 kW, which is shown by the red dashed curve in Fig. 2(b).

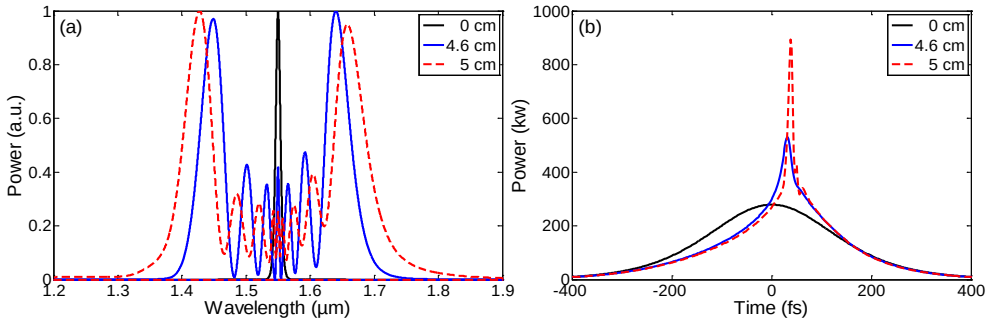

Fig. 2. Propagation of a 300-fs, 95-nJ pulse centered at 1.55 μm in an optical fiber with 10-μm MFD, –10 fs^2/mm GVD, and 100 fs^3/mm TOD at 1.55 μm. (a) spectra and (b) temporal pulses after propagation of 0-cm (black curves), 4.6-cm (blue curves), and 5-cm (red dashed curves).

Above results suggest that when implementing SESS using optical fibers with negative GVD, fiber length should be less than the soliton fission length to ensure SPM-dominated spectral broadening. Soliton fission length can be estimated as [38]

$$L_{fiss} \sim \frac{L_D}{N} = \frac{T_0^{\,2}/|\beta_2|}{\sqrt{\gamma E T_0/|\beta_2|}} = \sqrt{\frac{T_0^{\,3}}{|\beta_2|\gamma E}}, \quad (1)$$

where L_D is the characteristic dispersive length scale and N is the soliton order. T_0 is related to the full-width at half-maximum (FWHM) pulse duration by $T_0 \sim T_{\mathrm{FWHM}}/1.763$ assuming a hyperbolic-secant pulse. β_2 is the GVD, γ the nonlinear parameter of the optical fiber, and E the input pulse energy. In our simulation, these parameters are T_{FWHM} = 300 fs, β_2 = –10 fs^2/mm, γ = 1.73 /W/km, and E = 95 nJ, which result in L_{fiss} = 5.5 cm and agree well with the soliton fission length of 5.2 cm obtained by numerical simulation.

Equation (1) suggests that soliton fission length is inversely proportional to the square root of input pulse energy—a relation that favors SESS energy scaling. For example, as we quadruple the input pulse energy, the corresponding soliton fission length is reduced by half. Then we intuitively expect more accumulated nonlinear phase and a wider broadened spectrum. To numerically confirm such a speculation, we increase the input pulse energy from 95 nJ to 380 nJ, propagate the pulse in the fiber with –10 fs^2/mm GVD, and plot the spectral evolution in Fig. 3(b) for a fiber length up to 2.6 cm. For a clear comparison, Fig. 3(a) shows the spectral evolution for the input pulse with 95-nJ energy and the fiber length is set at 5.2 cm.

Optics EXPRESS

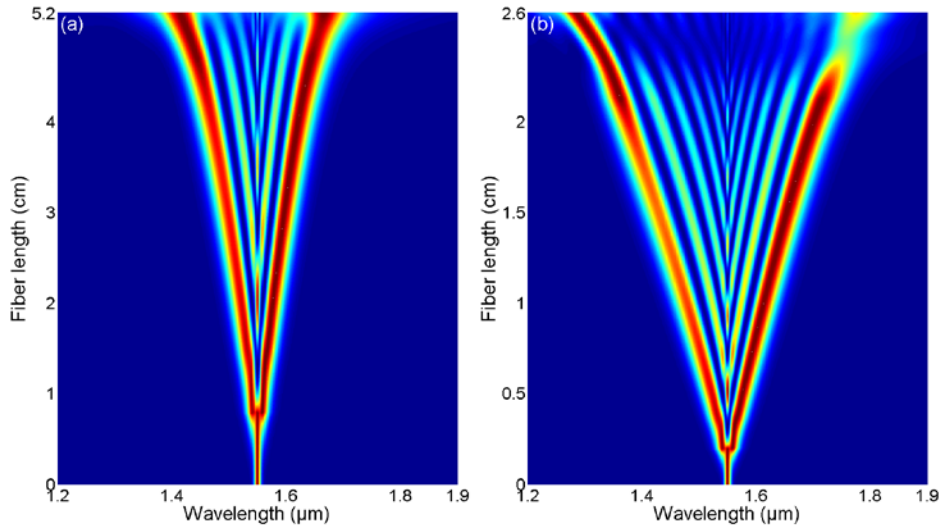

Fig. 3. Spectral evolution for different combinations of fiber length and input pulse energy: (a) 95-nJ pulse, fiber length up to 5.2 cm and (b) 380-nJ pulse, fiber length up to 2.6 cm. For both cases, the input pulse is a hyperbolic-secant pulse with 300-fs duration centered at 1.55 μm. The fiber has 10-μm MFD, –10 fs^2/mm GVD, and 100 fs^3/mm TOD at 1.55 μm.

Despite similar spectral evolution shown in Fig. 3(a) and 3(b), increasing the input pulse energy leads to a much wider SPM-dominated spectrum broadening. To illustrate this point, we plot in Fig. 4 the spectra and the pulses for different combinations of pulse energy and fiber length. For 95-nJ pulse energy and 4.6-cm fiber length, the blue curve in Fig. 4(a) shows that the leftmost and the rightmost spectral lobes peak at 1.45 μm and 1.64 μm, respectively. As we increase the pulse energy to 380 nJ and reduce the fiber length to 2.3 cm, these two lobes peak at 1.34 μm and 1.74 μm, shown by the red dashed curve in Fig. 4(a). The blue curve and the red dashed curve in Fig. 4(b) clearly indicate the higher-order soliton compression.

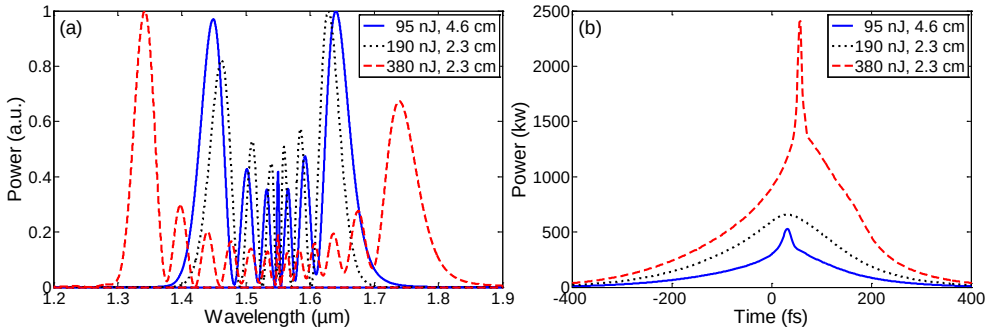

Fig. 4. (a) Spectral and (b) pulses for different combinations of fiber length and input pulse energy. blue curve: 95-nJ pulse, 4.6-cm fiber length, black dotted curve: 190-nJ pulse, 2.3-cm fiber length, and red dashed curve: 380-nJ pulse, 2.3-cm fiber length. The fiber has 10-μm MFD, –10 fs^2/mm GVD, and 100 fs^3/mm TOD at 1.55 μm.

For a better understanding of energy scaling, we also plot in Fig. 4 the simulation results corresponding to 190-nJ input pulse energy and 2.3-cm fiber length. From Eq. (1), we can estimate that the soliton fission length for the 190-nJ pulse is about 3.9 cm. As a result, propagation inside 2.3-cm fiber introduces negligible pulse compression [black dashed curve in Fig. 4(b)]. This explains why the resulting spectrum [black dashed curve in Fig. 4(a)] is

Optics EXPRESS

narrower than the one generated from 95-nJ pulse propagating in the 4.6-cm long fiber [blue curve in Fig. 4(a)]. Such behavior contrasts with SPM-dominated spectral broadening in a fiber with positive GVD, for which reducing the fiber length by a factor of 2 and doubling the input pulse energy leads to a wider broadened spectrum due to less pulse stretching [31–33].

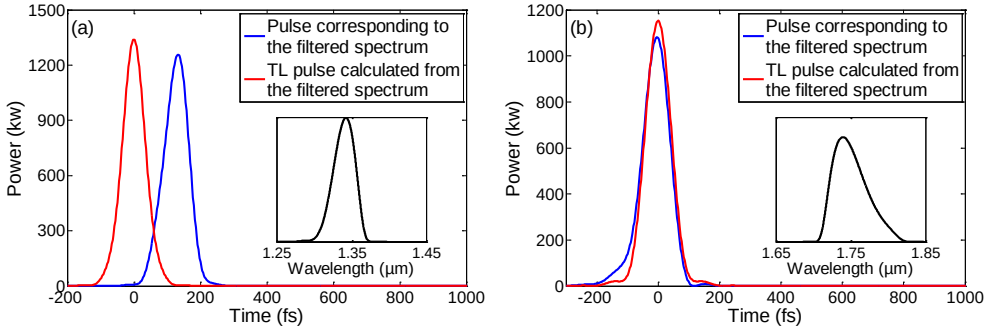

Fig. 5. Optical pulses (blue curves) and the calculated transform-limited (TL) pulses (red curves) from the filtered leftmost spectral lobe (a) and rightmost spectral lobe (b). These two spectral lobes are part of the SPM-dominated spectrum generated by propagating the 380-nJ pulse through 2.3-cm fiber. Insets: filtered optical spectra.

To demonstrate SESS, we numerically filter the leftmost and rightmost spectral lobes from the spectrum given by the 380-nJ pulse propagating through 2.3-cm fiber; the resulting pulses are plotted as the blue curves in Fig. 5. The filtered spectral lobes are shown as the black curves in the insets of Fig. 5. More specific, the filtered leftmost spectral lobe produces an 87-fs, 117-nJ pulse [blue curve in Fig. 6(a)], and the rightmost spectral lobe produces a 102-fs, 121-nJ pulse [blue curve in Fig. 6(b)]. Both pulses exhibit >1-MW peak power. The transform-limited pulses shown as the red curves in Fig. 6 calculated from the filtered spectra have durations of 78 fs and 98 fs, respectively, showing that the SESS pulses are nearly transform-limited. These two spectral lobes have a total pulse energy of 238 nJ, which accounts for >60% of the 380-nJ input pulse energy, representing an efficient wavelength conversion process.

3. Experimental results

Guided by above simulation results, we first use an Er-fiber laser as the driving source to experimentally implement such a SESS source in a fiber with negative GVD. The 31-MHz Er-fiber laser produces 290-fs pulses centered at 1.55 μm with up to 160-nJ pulse energy. More details about this Er-fiber laser system are presented in [33]. The optical fiber that we use in this paper is a dispersion-shifted fiber (DSF) with −10 fs^2/mm GVD and 10-μm MFD at 1.55 μm. Limited by the available pulse energy, we compare spectral evolution at two fiber lengths (14 cm versus 7 cm) that are longer than those in the simulation. Figure 6 shows the spectra at the output of the 14-cm DSF for the coupled pulse energy at 10 nJ, 15 nJ, 20 nJ, and 25 nJ. As the coupled pulse energy increases, the spectrum gradually broadens towards shorter and longer wavelength forming two isolated spectral lobes.

Optics EXPRESS

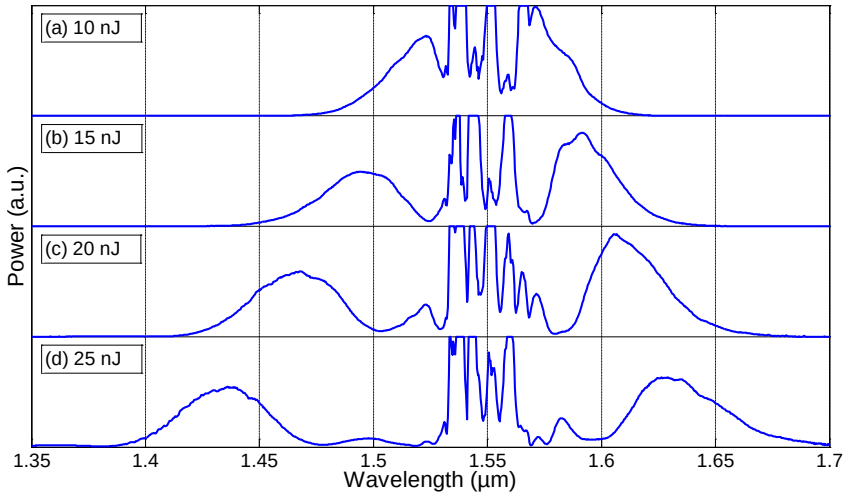

Fig. 6. Output spectra from 14-cm DSF with the coupled pulse energy of (a) 10 nJ, (b) 15 nJ, (c) 20 nJ, and (d) 25 nJ.

To investigate energy scaling by shortening the fiber length, we obtain SPM-dominated spectra at different combinations between fiber length and input pulse energy. Figure 7(a) plots the broadened spectrum of 28-nJ pulses by 14-cm DSF; the leftmost and rightmost spectral lobes peak at 1.42 μm and 1.64 μm, respectively. As we reduce the fiber length to 7 cm and increase the pulse energy to 56 nJ, the resulting spectrum shown in Fig. 7(b) experiences less broadening; the leftmost and rightmost spectral lobes peak at 1.44 μm and 1.62 μm, respectively. As we further increase the pulse energy to 112 nJ (4 times 28 nJ), spectral broadening in the 7-cm DSF shifts the leftmost spectral lobe to 1.32 μm and the rightmost one to 1.69 μm. Clearly the results shown in Fig. 7 qualitatively agree with the simulation results presented in Fig. 4(a).

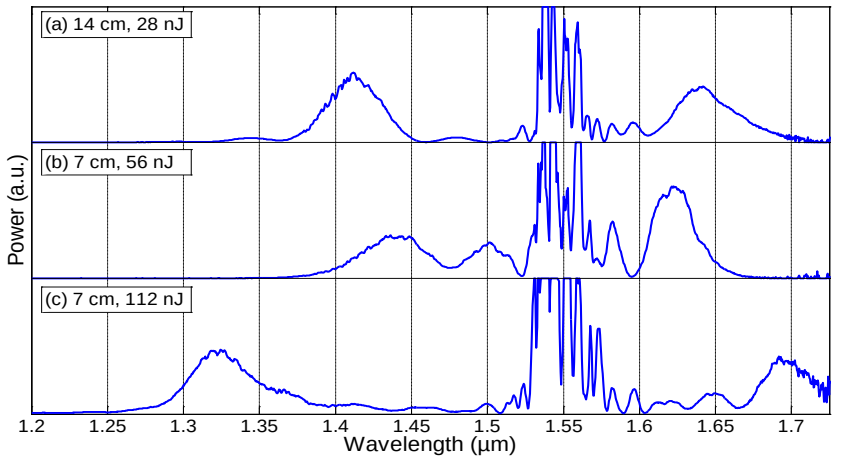

Fig. 7. Output spectra from DSF of different length and coupled pulse energy. (a) 14 cm, 28 nJ. (b) 7 cm, 56 nJ. (c) 7 cm, 112 nJ.

The experimental results in Fig. 7 indicate that energy scaling can be achieved by increasing the input pulse energy and meanwhile shortening the fiber length. The peak wavelength of the leftmost and rightmost spectral lobes can be continuously tuned by varying the coupled pulse energy. For example, SPM-dominated spectral broadening in the 7-cm DSF

Optics EXPRESS

followed by optical filters to select the leftmost/rightmost spectral lobes results in a femtosecond source with the wavelength tunable between 1.3 μm and 1.7 μm.

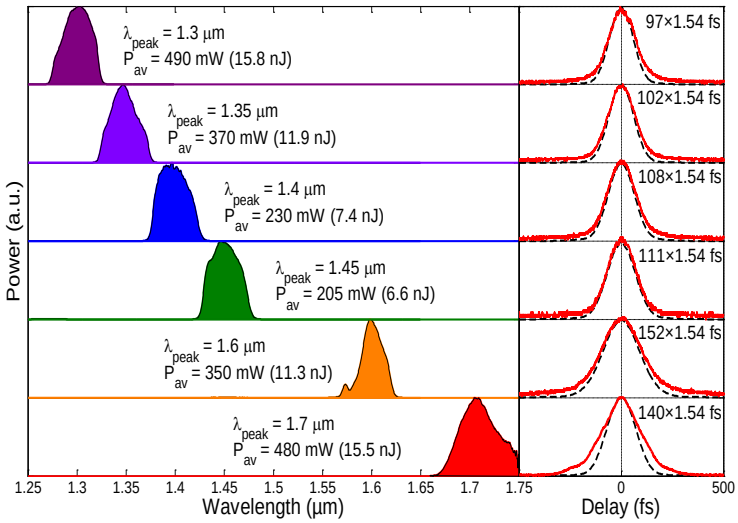

Fig. 8. (Left column) Filtered optical spectra from 7-cm DSF; their peak wavelength, average power, and pulse energy are labeled in the figure. (Right column) Measured autocorrelation traces (red solid curves) and autocorrelation traces calculated from the transform-limited pulses allowed by the filtered spectra (black dashed curves).

To show the wavelength tunability, we plot 6 representative filtered spectral lobes in the left column of Fig. 8. They peak at 1.3 μm, 1.35 μm, 1.4 μm, 1.45 μm, 1.6 μm, and 1.7 μm with the corresponding pulse energy of 15.8 nJ, 11.9 nJ, 7.4 nJ, 6.6 nJ, 11.3 nJ, and 15.5 nJ, respectively. At 31-MHz repetition rate, this tunable femtosecond source has an average power of 230-490 mW. The corresponding pulses given by these 6 spectra are measured by an intensity autocorrelator and the measured autocorrelation traces are shown as the red solid curves in the right column of Fig. 8. The FWHM duration of these autocorrelation traces is 149-234 fs. The pulse duration is estimated to be 97-152 fs assuming a hyperbolic-secant pulse with a deconvolution factor of 1.54. The black dashed curves in the right column plot the calculated autocorrelation traces of the transform-limited pulses allowed by the filtered spectra, showing that the filtered spectra generate nearly transform-limited pulses.

It is noteworthy that the filtered spectra at 1.3 μm and 1.7 μm are obtained from the same broadened spectrum corresponding to 115-nJ coupled pulse energy. The total pulse energy distributed in the leftmost and the rightmost spectral lobes is 31.3 nJ, corresponding to 27% energy conversion efficiency. In our previous work, we used the same laser source to derive SESS sources based on positive-GVD fibers [33]. By also coupling 115-nJ pulses into 4-cm dispersion-compensating fiber with 48.5 fs^2/mm GVD at 1.55 μm, the resulting leftmost and rightmost spectral lobes peak at 1.35 μm and 1.7 μm, respectively [33]. The total pulse energy given by these two spectral lobes is 21 nJ, accounting for 18% energy conversion efficiency. Apparently SESS based on negative-GVD fibers exhibits a better energy scalability.

The filtered spectra at 1.3 μm and 1.7 μm correspond to two important optical windows for biomedical imaging [34]. Femtosecond pulses at these two wavelengths are regarded as the best choice for deep-tissue imaging [35,36]. Depending on the biological sample and the imaging modality, femtosecond pulses with MW peak power may be desired [35,36]. Limited by the available pulse energy of 160 nJ provided by the Er-fiber laser system, the SESS source based on 7-cm DSF produces ~100-fs pulses with ~16-nJ pulse energy at both 1.3 μm and 1.7 μm. The resulting peak power is at the 0.1 MW level. To show the feasibility of

Optics EXPRESS

further energy scaling, we replace the Er-fiber laser system by a home-built OPA system that is pumped by a 3-kHz Ti:sapphire laser.

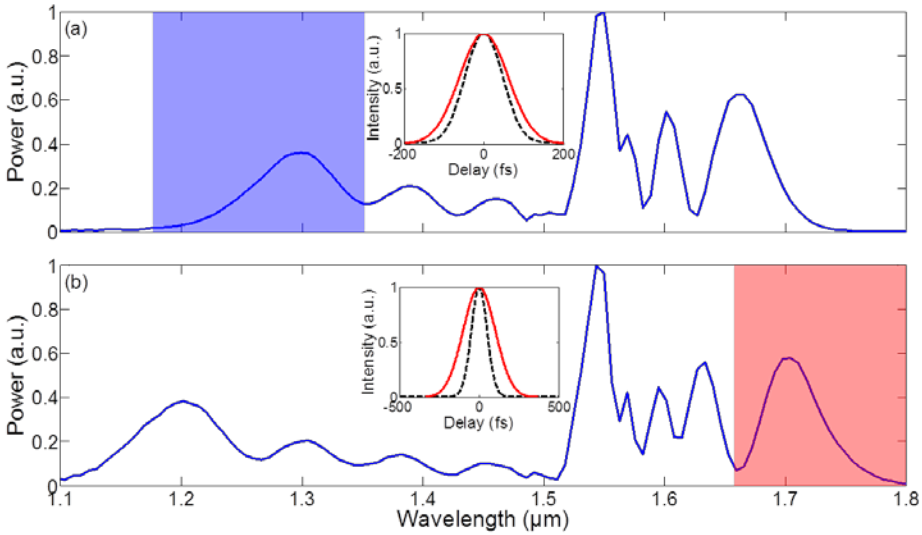

Fig. 9. MW peak power SESS source at (a) 1.3 μm and (b) 1.7 μm. The whole spectra are generated by SPM-dominated spectral broadening in 1.3-cm DSF. The input narrowband 1.55 μm pulses are produced by a home-built OPA. Insets: the measured autocorrelation traces (red curves) for the filtered spectral lobes (shaded part of the whole spectrum). Black dashed curves show the calculated autocorrelation traces of the transform-limited pulses given by the filtered spectra.

The signal pulse from the OPA is tunable between 1.2 μm and 1.6 μm with ~40-fs pulse duration. To match the pulse parameters of our Er-fiber laser system, we intentionally tune the signal wavelength to 1.55 μm and use an optical bandpass filter to select a narrowband spectrum that supports ~300-fs pulses. We couple this narrowband pulse into 1.3-cm DSF. By varying the input pulse energy, we can fine tune the peak position of the leftmost/rightmost spectral lobes. At the 760-nJ coupled pulse energy, the measured spectrum plotted in Fig. 9(a) shows that the leftmost spectral lobe peaks at 1.3 μm. We use an optical filter to select this spectral lobe and obtain 130-nJ pulse energy. The resulting pulse is measured by an intensity autocorrelator. The measured autocorrelation trace—shown as the red curve in the inset of Fig. 9(a)—suggests a 94-fs pulse duration assuming a deconvolution factor of 1.54. The black dashed curve represents the calculated autocorrelation trace for the transform-limited pulse. Given 130-nJ pulse energy and estimated pulse duration of 94 fs, the pulse peak power should exceed 1 MW. To shift the rightmost spectral lobe to 1.7 μm [Fig. 9(b)], we increase the input pulse energy to 830 nJ. The filtered pulse at 1.7 μm has 110-nJ pulse energy and an estimated pulse duration of 150 fs [inset of Fig. 9(b)]. The resulting peak power is at the MW level. It is worth noting that the leftmost spectral lobe in Fig. 9(b) peaks at 1.2 μm. Filtering this spectral lobe should also lead to ~100-fs pulses with ~100 nJ pulse energy.

4. Conclusion

We present a detailed numerical and experimental study on SESS in optical fibers with different dispersion. Although spectral broadening inside optical fibers with negative GVD involves higher-order soliton compression and soliton fission, our results show that SPM dominates the spectral broadening prior to soliton fission. Before soliton fission occurs, higher-order soliton compression increases the pulse peak power and accelerates the spectral broadening. The broadened spectrum features two well-isolated spectral lobes whose peak wavelengths can be continuously tuned by varying the input pulse energy. The SESS source

Optics EXPRESS

as a result of filtering the leftmost/rightmost spectral lobes can produce energetic ~100-fs pulses. Using 7-cm DSF to broaden the spectrum offered by an ultrafast Er-fiber laser, we implement a SESS source that can be tuned from 1.3 μm to 1.7 μm with up to ~16-nJ pulse energy. By increasing the input pulse energy to ~1-μJ (offered by an OPA source) and reducing the DSF length to 1.3 cm, we significantly scale up the pulse energy of such a SESS source. More specific, we achieve >100-nJ femtosecond pulses at 1.3 μm and 1.7 μm while the peak power reaches the MW level.

Currently we are employing the Er-fiber laser enabled SESS source to perform multiphoton deep-tissue imaging. Meanwhile, we are also upgrading our Er-fiber laser to the ~1-μJ level to implement an Er-fiber laser based SESS source that produces widely tunable femtosecond pulses with MW peak power. We believe such a powerful source will open many new applications.

Funding

Helmholtz Young Investigator Group (VH-NG-804); Helmholtz-CAS Joint Research Group (HCJRG 201); The Hamburg Centre for Ultrafast Imaging—Structure, Dynamics and Control of Matter at the Atomic scale of the Deutsche Forschungsgemeinschaft (EXC 1074).